Adaptive Element-Free Galerkin method applied to the limit analysis of plates

Canh V. Le [a], Harm Askes [a,*] and Matthew Gilbert [a]

[a] *University of Sheffield, Department of Civil and Structural Engineering, Sheffield S1 3JD, United Kingdom*

Abstract

The implementation of an h-adaptive Element-Free Galerkin (EFG) method in the framework of limit analysis is described. The naturally conforming property of meshfree approximations (with no nodal connectivity required) facilitates the implementation of h-adaptivity. Nodes may be moved, discarded or introduced without the need for complex manipulation of the data structures involved. With the use of the Taylor expansion technique, the error in the computed displacement field and its derivatives can be estimated throughout the problem domain with high accuracy. A stabilized conforming nodal integration scheme is extended to error estimators and results in an efficient and truly meshfree adaptive method. To demonstrate its effectiveness the procedure is then applied to plates with various boundary conditions.

Key words: Error estimation, adaptivity, limit analysis, EFG method, second-order cone programming

1 INTRODUCTION

Limit analysis makes use of the fundamental theorems of plastic analysis to provide a powerful means of estimating the maximum load sustainable by a solid or structure. Mathematical programming techniques can often be applied to permit the collapse load to be determined directly. In recent years efforts have focussed principally on the development of efficient and robust numerical

* Corresponding author
Email addresses: Canh.Le@sheffield.ac.uk (Canh V. Le), h.askes@sheffield.ac.uk (Harm Askes), m.gilbert@sheffield.ac.uk (Matthew Gilbert).

limit analysis tools of potential use to engineers working in practice, which either use continuous (e.g. using finite element [1–7] or meshless [8–10] methods), semi-continuous [11] or truly discontinuous [12] representations of the relevant field variables. However, the accuracy of numerical limit analysis solutions is highly affected by local singularities arising from localized plastic deformations [13]. In order to achieve accurate solutions automatic h-refinement is often performed, so that the resolution of the spatial discretization is refined in plastic zones. Automatic finite element mesh refinement based on both stress and strain fields has been previously proposed [14], where elements are candidates for refinement if the strain tensor is non-zero. Alternatively, adaptive procedures based on *a posteriori* error estimates to measure the local and global errors associated with the interpolation have been developed for limit analysis problems. A directional error estimate using recovery gradients and/or the Hessian of mixed finite element solutions was proposed in [13]. The scheme was then adapted to lower bound limit analysis by using quasi-velocities and plastic multipliers from the dual solution [15]. Using solutions of the lower and upper bound problem in combination, another effective error estimate was proposed in [16,17]. These techniques have been used successfully for various 2D problems.

Meshfree methods are very attractive computational techniques due to their flexibility, e.g. no nodal connectivity is required. The naturally conforming property of meshfree approximations offers considerable advantages in adaptive analysis. Nodes can easily be added and removed without the need for complex manipulation of the data structures involved. Since error estimates for finite elements are not always directly transferable to meshfree methods, various approaches have been proposed [18–23]. Effective approaches to estimate the interpolation/approximation error were proposed in [20, 21, 24, 25]. The approximation error in the computed displacement field and its derivatives can be evaluated with high accuracy using a Taylor expansion of the relevant field variable. It is also shown in [21] that this estimate is generally suitable for problems with high stress and strain gradients and singularities. While these approaches have been developed for structured meshfree particle methods using Gauss integration, it is also desirable to develop an efficient method for general irregular nodal layouts. In this paper the error density in a representative nodal cell can be determined using smoothed values of the displacement derivatives. This not only results in a truly meshfree method but also reduces the effort required to calculate displacement derivatives in the error estimate. Furthermore, since the Voronoi diagram for a set of nodes is unique, properties of Voronoi cells can be conveniently used as a reference for refinement strategies and for determining locally the size of the domain of influence.

In the framework of meshfree methods, it is advantageous if the problem under consideration can be solved by evaluating quantities at the nodes only [26–32].

The smoothing technique proposed in [28] is one of the most efficient nodal integration methods available, and has been applied successfully to various analysis problems [9, 10, 33–35]. In this technique nodal values are determined by spatially averaging field values using the divergence theorem. In other words, the domain integrals are transformed into boundary integrals to avoid the evaluation of the derivatives of the meshfree shape functions at the nodes, where they vanish, thus eliminating spatial instability problems. In this paper the range of applicability of the smoothing technique is extended by applying it to a kinematic limit analysis formulation incorporating error estimation.

The objective of this paper is to develop a meshfree h-adaptivity procedure for limit analysis problems. The layout of the paper is as follows: Section 2 briefly describes a kinematic upper bound limit analysis formulation for plates using the Element-Free Galerkin (EFG) method and stabilized conforming nodal integration (SCNI). A cell-based error estimate for the displacement field and its derivatives is presented in Section 3. Based on the error estimate discussed in Section 3, error indicators and refinement strategies are introduced in Section 4. Numerical examples are provided in Section 5 to illustrate the performance of the proposed procedure.

2 LIMIT ANALYSIS OF PLATES - DISCRETE KINEMATIC FORMULATION

In this section the kinematic formulation for the plate limit analysis problem is outlined, together with details of the EFG method and the second-order cone programming (SOCP) problem formulation. More details can be found in [9].

Consider a rigid-perfectly plastic plate governed by the von Mises yield criterion, subjected to a distributed load $\alpha^+ q$ and with a constrained boundary Γ_u. The upper bound limit analysis problem for plates can be written as

$$\alpha^+ = \min \int_\Omega m_p \, \|\mathbf{C}^T \, \dot{\boldsymbol{\kappa}}\|_{L^2(\Omega)} \, \mathrm{d}\Omega \tag{1a}$$

$$\text{s.t}$$

$$\dot{\boldsymbol{\kappa}} = -\left\{ \frac{\partial^2 \dot{u}^h}{\partial x^2} \;\; \frac{\partial^2 \dot{u}^h}{\partial y^2} \;\; 2\frac{\partial^2 \dot{u}^h}{\partial x \partial y} \right\}^T \tag{1b}$$

$$\int_\Omega q u^h \, \mathrm{d}\Omega = 1 \tag{1c}$$

accompanied by appropriate boundary conditions, where q is unit load per area, α^+ is a scalar collapse load multiplier, $m_p = \sigma_0 t^2/4$ is the plastic moment of resistance per unit width of a plate of thickness t and $\mathbf{C}$ is a matrix that

depends on the yield criterion involved. For the von Mises criterion,

$$\mathbf{C} = \frac{1}{\sqrt{3}} \begin{bmatrix} 2 & 0 & 0 \\ 1 & \sqrt{3} & 0 \\ 0 & 0 & 1 \end{bmatrix} \tag{2}$$

The approximated transverse displacement $u^h(\mathbf{x})$ is computed using a Moving Least Squares (MLS) technique and is expressed as

$$u^h(\mathbf{x}) = \sum_{I=1}^{n} \Phi_I(\mathbf{x}) u_I \tag{3}$$

The MLS shape functions $\Phi_I(\mathbf{x})$ are given as [36, 37]

$$\Phi_I(\mathbf{x}) = \mathbf{p}^T(\mathbf{x}) \mathbf{A}^{-1}(\mathbf{x}) \mathbf{B}_I(\mathbf{x}) \tag{4}$$

with

$$\mathbf{A}(\mathbf{x}) = \sum_{I=1}^{n} w_I(\mathbf{x}) \mathbf{p}(\mathbf{x}_I) \mathbf{p}^T(\mathbf{x}_I) \tag{5}$$

$$\mathbf{B}_I(\mathbf{x}) = w_I(\mathbf{x}) \mathbf{p}(\mathbf{x}_I) \tag{6}$$

where n is the number of nodes; $\mathbf{p}(\mathbf{x}) = [1, x, y, xy, x^2, y^2]^T$ is a quadratic basis function and $w_I(\mathbf{x})$ is an isotropic quartic spline weight function associated with node I.

Introducing stabilized conforming nodal integration [28], smoothed curvature rates $\dot{\boldsymbol{\kappa}}(\mathbf{x}_j)$ at nodal point $\mathbf{x}_j$ are written as

$$\dot{\boldsymbol{\kappa}}(\mathbf{x}_j) = -\mathbf{G}\ \mathbf{v} \tag{7}$$

where

$$\mathbf{v}^T = [\dot{u}_1,\ \dot{u}_2,\ \ldots\ , \dot{u}_n] \tag{8}$$

$$\mathbf{G} = \begin{bmatrix} \tilde{\Phi}_{1,xx}(\mathbf{x}_j) & \tilde{\Phi}_{2,xx}(\mathbf{x}_j) & \ldots & \tilde{\Phi}_{n,xx}(\mathbf{x}_j) \\ \tilde{\Phi}_{1,yy}(\mathbf{x}_j) & \tilde{\Phi}_{2,yy}(\mathbf{x}_j) & \ldots & \tilde{\Phi}_{n,yy}(\mathbf{x}_j) \\ 2\tilde{\Phi}_{1,xy}(\mathbf{x}_j) & 2\tilde{\Phi}_{2,xy}(\mathbf{x}_j) & \ldots & 2\tilde{\Phi}_{n,xy}(\mathbf{x}_j) \end{bmatrix} \tag{9}$$

with

$$\begin{aligned}\tilde{\Phi}_{I,\alpha\beta}(\mathbf{x}_j) &= \frac{1}{2a_j}\oint_{\Gamma_j}\left(\Phi_{I,\alpha}(\mathbf{x}_j)n_\beta(\mathbf{x}) + \Phi_{I,\beta}(\mathbf{x}_j)n_\alpha(\mathbf{x})\right)\mathrm{d}\Gamma \\ &= \frac{1}{4a_j}\sum_{k=1}^{ns}\left(n_\beta^k\, l^k + n_\beta^{k+1}\, l^{k+1}\right)\Phi_{I,\alpha}(\mathbf{x}_j^{k+1}) \\ &+ \frac{1}{4a_j}\sum_{k=1}^{ns}\left(n_\alpha^k\, l^k + n_\alpha^{k+1}\, l^{k+1}\right)\Phi_{I,\beta}(\mathbf{x}_j^{k+1}) \end{aligned} \tag{10}$$

where $\tilde{\Phi}$ is the smoothed version of Φ; a_j, Γ_j and ns are respectively the area, boundary and the number of segments of a Voronoi nodal domain Ω_j as shown in the Figure 1; $\mathbf{x}_j^k$ and $\mathbf{x}_j^{k+1}$ are the coordinates of the two end points of boundary segment Γ_j^k which has length l^k and outward surface normal n^k.

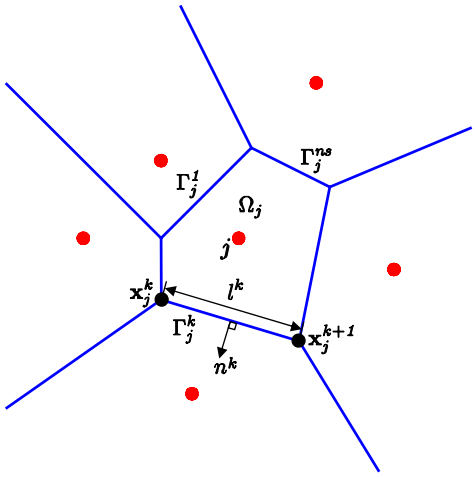

Fig. 1. Geometry of a representative nodal domain

The kinematic limit analysis problem for plates can now be written in the form of a SOCP problem as follows:

$$\alpha^+ = \min \;\; m_p \sum_{j=1}^{n} a_j t_j \tag{11a}$$

s.t

$$\mathbf{A}_{eq}\mathbf{v} = \mathbf{b}_{eq} \tag{11b}$$

$$-\mathbf{C}^T\mathbf{G}\mathbf{v} = \mathbf{r}_i \tag{11c}$$

$$\| \mathbf{r}_i \| \leq t_i, \quad i = 1, 2, \ldots, n \tag{11d}$$

in which Eq. (11d) expresses quadratic cones and $\mathbf{r}_i \in \mathbb{R}^3$ are additional variables defined by Eq. (11c), where every $\mathbf{r}_i$ is a 3×1 vector. Matrix $\mathbf{A}_{eq}$ and vector $\mathbf{b}_{eq}$ are obtained from unitary external work Eq. (1c) and boundary

conditions, and they are given by

$$\mathbf{A}_{eq} = \begin{bmatrix} \sum_{j=1}^{n} a_j \Phi_1(\mathbf{x}_j) & \sum_{j=1}^{n} a_j \Phi_2(\mathbf{x}_j) & \dots & \sum_{j=1}^{n} a_j \Phi_n(\mathbf{x}_j) \\ \Phi_1(\mathbf{x}_1^b) & \Phi_2(\mathbf{x}_1^b) & \dots & \Phi_n(\mathbf{x}_1^b) \\ \vdots & \vdots & \ddots & \vdots \\ \Phi_1(\mathbf{x}_d^b) & \Phi_2(\mathbf{x}_d^b) & \dots & \Phi_n(\mathbf{x}_d^b) \\ \Phi_{1,x}(\mathbf{x}_1^b) & \Phi_{2,x}(\mathbf{x}_1^b) & \dots & \Phi_{n,x}(\mathbf{x}_1^b) \\ \vdots & \vdots & \ddots & \vdots \\ \Phi_{1,x}(\mathbf{x}_{rx}^b) & \Phi_{2,x}(\mathbf{x}_{rx}^b) & \dots & \Phi_{n,x}(\mathbf{x}_{rx}^b) \\ \Phi_{1,y}(\mathbf{x}_1^b) & \Phi_{2,y}(\mathbf{x}_1^b) & \dots & \Phi_{n,y}(\mathbf{x}_1^b) \\ \vdots & \vdots & \ddots & \vdots \\ \Phi_{1,y}(\mathbf{x}_{ry}^b) & \Phi_{2,y}(\mathbf{x}_{ry}^b) & \dots & \Phi_{n,y}(\mathbf{x}_{ry}^b) \end{bmatrix} \tag{12}$$

$$\mathbf{b}_{eq}^T = \begin{bmatrix} 1 \overbrace{0\ 0 \dots 0}^{d} \overbrace{0\ 0 \dots 0}^{rx} \overbrace{0\ 0 \dots 0}^{ry} \end{bmatrix} \tag{13}$$

Here d is the number of boundary nodes having displacement conditions and rx and ry are the number of boundary nodes having rotation conditions about x and y, respectively. It is noted that tangential rotations along the boundary are also enforced as this has been found to increase the accuracy of the solutions.

3 ESTIMATION OF APPROXIMATION ERRORS

A key ingredient of any adaptive analysis procedure is the formulation of an error estimate which determines which parts of the domain are most in need of refinement. Here we will use the error estimate approach given in [20,21,24,25]. The estimated error for general approximations of s^{th} order completeness is presented first, from which the error for linear and quadratic cases in 2D can be retrieved. An approximation is complete to order s if any polynomial up to order s is exactly reproduced as

$$\sum_{I=1}^{n} x^p \Phi_I(\mathbf{x}) = x^p \quad \text{for} \quad 0 \leq p \leq s \tag{14}$$

The error can be written as

$$u^h(\mathbf{x}) - u(\mathbf{x}) = \sum_{I=1}^{n} \Phi_I(\mathbf{x}) u_I - u(\mathbf{x}) \tag{15}$$

Expanding $u(\mathbf{x})$ by a Taylor series, the nodal values of the exact solution are indicated as $u(\mathbf{x}_I)$ and can be expressed as

$$u(\mathbf{x}_I) = \sum_{m=0}^{s} \frac{1}{m!} \left((x_I - x)\frac{\partial}{\partial x} + (y_I - y)\frac{\partial}{\partial y} + (z_I - z)\frac{\partial}{\partial z} \right)^m u(\mathbf{x}) + R_{s+1} \tag{16}$$

with

$$R_{s+1} = \frac{1}{(s+1)!} \left((x_I - x)\frac{\partial}{\partial x} + (y_I - y)\frac{\partial}{\partial y} + (z_I - z)\frac{\partial}{\partial z} \right)^{s+1} u(\bar{\mathbf{x}}),$$
$$\bar{\mathbf{x}} = (1-\nu)\mathbf{x} + \nu \mathbf{x}_I,\ 0 < \nu < 1 \tag{17}$$

Combining the conditions of an approximation of s^{th} order completeness with Eqs. (15,16), the approximation error reads

$$u^h(\mathbf{x}) - u(\mathbf{x}) = \frac{1}{(s+1)!} \left((x_I - x)\frac{\partial}{\partial x} + (y_I - y)\frac{\partial}{\partial y} + (z_I - z)\frac{\partial}{\partial z} \right)^{s+1} u(\bar{\mathbf{x}}) \tag{18}$$

The shape functions are bounded, that is $|\Phi(\mathbf{x})| \leq c$ where c is a bounded constant, and have compact support ($|x_I - x| \leq h_I$, $|y_I - y| \leq h_I$ and $|z_I - z| \leq h_I$). Defining

$$D = \left(\frac{\partial}{\partial x} + \frac{\partial}{\partial y} + \frac{\partial}{\partial z} \right) \tag{19}$$

and taking the L^2-norm of the error estimate, Eq. (18) becomes

$$\|u^h(\mathbf{x}) - u(\mathbf{x})\|_{L^2(\Omega)} = c h_I^{s+1} \left\| \frac{1}{(s+1)!} D^{s+1} u \right\|_{L^2(\Omega)} \tag{20}$$

Similarly, the approximation error associated with the derivatives can be estimated. The error in the first derivative is expressed as

$$\left\| \frac{\partial u^h(\mathbf{x})}{\partial \mathbf{x}} - \frac{\partial u(\mathbf{x})}{\partial \mathbf{x}} \right\|_{L^2(\Omega)} = c h_I^{s} \left\| \frac{1}{(s+1)!} D^{s+1} u \right\|_{L^2(\Omega)} \tag{21}$$

For 2D problems, the approximation error of the first derivative is

$$\left\| \frac{\partial u^h(\mathbf{x})}{\partial \mathbf{x}} - \frac{\partial u(\mathbf{x})}{\partial \mathbf{x}} \right\|_{L^2(\Omega)} = c h_I \left\| \frac{1}{2} \left(u_{,xx} + u_{,yy} + 2u_{,xy} \right) \right\|_{L^2(\Omega)} \tag{22}$$

for a linear basis function, and it is

$$\left\| \frac{\partial u^h(\mathbf{x})}{\partial \mathbf{x}} - \frac{\partial u(\mathbf{x})}{\partial \mathbf{x}} \right\|_{L^2(\Omega)} = ch_I^2 \left\| \frac{1}{6} \left(u_{,xxx} + u_{,yyy} + 3 \left(u_{,xxy} + u_{,yyx} \right) \right) \right\|_{L^2(\Omega)} \tag{23}$$

for a quadratic basis function.

4 ADAPTIVE PROCEDURE

4.1 Updating the shape functions

In meshfree adaptive analysis, new nodes are added in those parts of the domain where the error exceeds a predefined tolerance. These new nodes locally impact on the shape functions of neighbouring nodes. In order to reduce computational cost and to ensure consistency of the MLS approximation, matrix $\mathbf{A}$ in the shape functions of existing nodes are reconstructed locally as [22]:

$$\begin{aligned} \mathbf{A}(\mathbf{x}) &= \sum_{I=1}^{n_{old}} w_I(\mathbf{x}) \mathbf{p}(\mathbf{x}_I) \mathbf{p}^T(\mathbf{x}_I) + \sum_{I=1}^{n_{new}} w_I(\mathbf{x}) \mathbf{p}(\mathbf{x}_I) \mathbf{p}^T(\mathbf{x}_I) \\ &= \mathbf{A}_{old}(\mathbf{x}) + \sum_{I=1}^{n_{new}} w_I(\mathbf{x}) \mathbf{p}(\mathbf{x}_I) \mathbf{p}^T(\mathbf{x}_I) \end{aligned} \tag{24}$$

This is illustrated with a one-dimensional example in Figure 2, where an added node 12 can be seen to affect the shape functions of nodes 6 and 7.

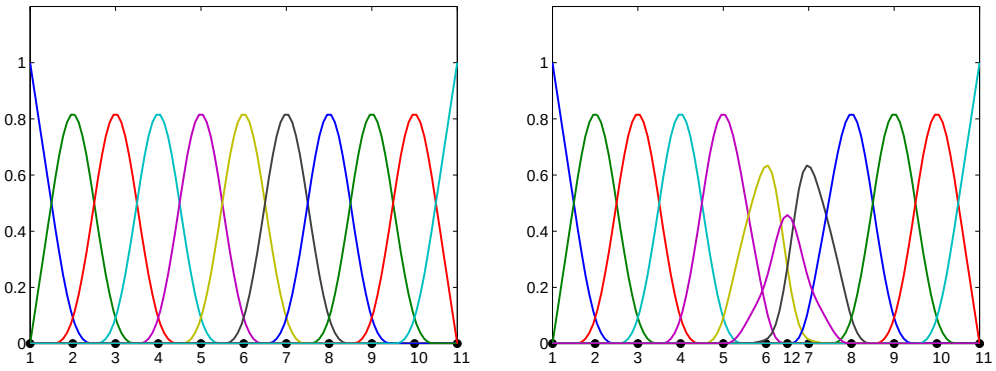

(a) Before adaptivity (b) After adaptivity

Fig. 2. Nodal refinement strategies based on Voronoi cells

Note that in an adaptive refinement procedure nodes will often be distributed irregularly. Therefore the size of the domain of influence needs to be determined locally. The Voronoi diagram for a set of nodes is unique, and from

the Voronoi cell information, the neighbours of node I can be identified and grouped as N_I, as shown in Figure 3

$$\begin{aligned} N_I &= \{P_J : V(P_J) \cap V(P_I) \neq \oslash\} \\ &= \{p_1, p_2, p_3, p_4, p_5, p_6, p_7\} \end{aligned} \tag{25}$$

where $V(P_I)$ is the Voronoi cell of particle P_I.

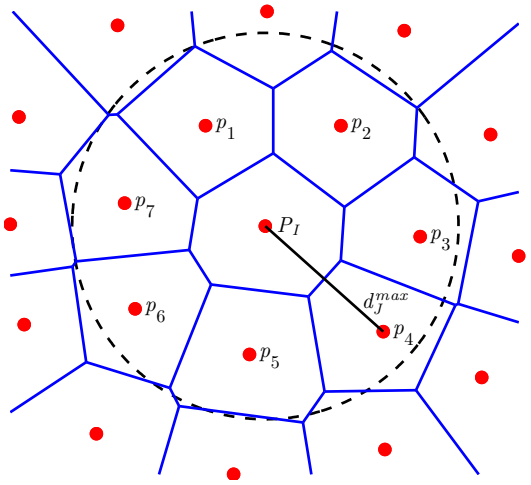

Fig. 3. Determination of shape function support size

The size of the domain of influence of node I is then determined as

$$h_I = \beta \cdot \max\{d_J : d_J = \overline{P_I P_J},\ \forall P_J \in N_I\} \tag{26}$$

4.2 Refinement criteria

Based on the error estimate discussed in Section 3, the local error is computed for each integration cell from the displacement fields obtained by solving the optimization problem. This local error is controlled as follows

$$h_I^s \left\| \frac{1}{(s+1)!} D^{s+1} u \right\|_{L^2(\Omega)} \leq \delta \tag{27}$$

where δ is a dimensionless user-defined error tolerance value which will be discussed in more detail in Section 5.

It is important to note that it is often computationally expensive to calculate the terms $D^{s+1}u$ in Eq. (27), especially for problems using second, or higher, order basis functions. Furthermore, in order to evaluate accurately the LHS term in Eq. (27) a large number of Gauss points would be needed [21]. The

smoothing technique proposed in [28] can be extended to overcome this difficulty. Introducing smoothing of $D^{s+1}u(\mathbf{x})$ at a representative nodal domain Ω_j, we have

$$D^{s+1}\tilde{u}(\mathbf{x}_j) = \frac{1}{a_j}\int_{\Omega_j} D^{s+1}u(\mathbf{x})\mathrm{d}\Omega \tag{28}$$

Introducing now the MLS approximation of the displacement field, we obtain

$$D^{s+1}\tilde{u}(\mathbf{x}_j) = \sum_{I=1}^{n} D^{s+1}\tilde{\Phi}_I(\mathbf{x}_j)u_I \tag{29}$$

where

$$D^{s+1}\tilde{\Phi}_I(\mathbf{x}_j) = \frac{1}{a_j}\int_{\Omega_j} D^{s+1}\Phi_I(\mathbf{x})\mathrm{d}\Omega \tag{30}$$

With the use of this smoothing technique, the cell-based error tolerance can be rewritten as

$$a_j h_j^s \left|\left| \frac{1}{(s+1)!} D^{s+1}\tilde{u}(\mathbf{x}_j) \right|\right|_{L^2(\Omega_j)} \leq \delta \tag{31}$$

The global error estimator is the sum of the local errors of all cells and is given by

$$||e||_{L^2(\Omega)} = \left(\sum_{j=1}^{n} \left(a_j h_j^s \left|\left| \frac{1}{(s+1)!} D^{s+1}\tilde{u}(\mathbf{x}_j) \right|\right|_{L^2(\Omega_j)} \right)^2 \right)^{1/2} \tag{32}$$

For plate problems, quadratic basis functions must be used [38]. The local cell-based error estimator then reads

$$a_j h_j^2 \left|\left| \frac{\tilde{u}_{,xxx}(\mathbf{x}_j) + \tilde{u}_{,yyy}(\mathbf{x}_j) + 3\left(\tilde{u}_{,xxy}(\mathbf{x}_j) + \tilde{u}_{,yyx}(\mathbf{x}_j)\right)}{6} \right|\right|_{L^2(\Omega_j)} \leq \delta \tag{33}$$

in which

$$\tilde{u}_{,\alpha\alpha\beta}(\mathbf{x}_j) = \sum_{I=1}^{n} \tilde{\Phi}_{I,\alpha\alpha\beta}(\mathbf{x}_j)u_I \tag{34}$$

$$\tilde{\Phi}_{I,\alpha\alpha\beta}(\mathbf{x}_j) = \frac{1}{2a_j}\oint_{\Gamma_j} \left(\Phi_{I,\alpha\alpha}(\mathbf{x}_j)n_\beta(\mathbf{x}) + \Phi_{I,\alpha\beta}(\mathbf{x}_j)n_\alpha(\mathbf{x})\right)\mathrm{d}\Gamma \tag{35}$$

The technique used to determine the boundary integral in Eq. (10) can be applied here to evaluate the term on the RHS of Eq. (35).

4.3 Refinement strategy

The problem domain is subdivided into nodes and an associated Voronoi diagram is constructed. If the local error in a Voronoi cell exceeds the predefined value δ, new nodes are added as shown in Figure 4 [22, 23]. It can be seen from the figure that the cells in the Voronoi diagram resulting from strategy

(I) are more uniformly sized than those resulting from strategy (II), and also that the number of nodes added in the two cases is identical.

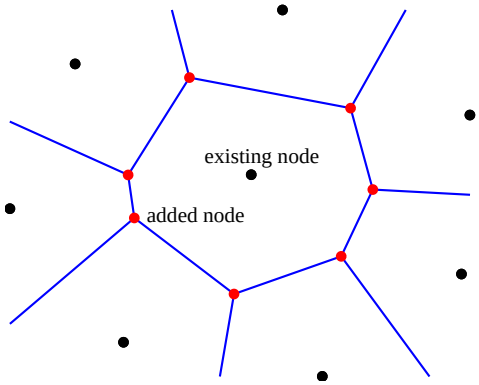

(a) Strategy I: adding nodes on vertices of Voronoi cell

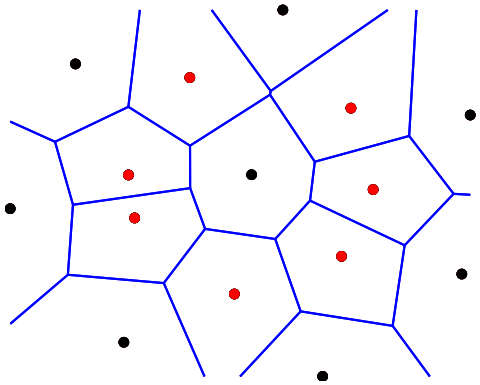

(b) Voronoi cells associated with (a)

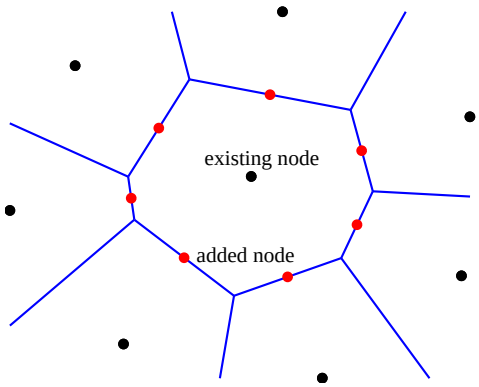

(c) Strategy II: adding midpoint nodes on edges of Voronoi cell

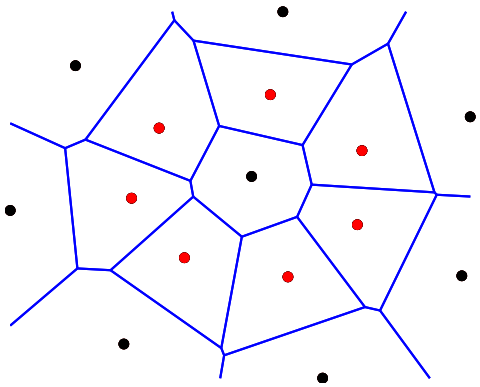

(d) Voronoi cells associated with (c)

Fig. 4. Nodal refinement strategies based on Voronoi cells (added nodes shown in red)

The efficiency of these refinement strategies will be discussed in the next section. The adaptive procedure can be summarised as follows:

5 NUMERICAL EXAMPLES

The efficacy of the proposed adaptive meshfree procedure for limit analysis problems will now be demonstrated by applying it to plate problems of various geometries and loaded by either a uniform pressure or concentrated forces. For all the examples considered the following parameters were assumed: plate thickness $t = 0.1$ m; yield stress $\sigma_0 = 250$ MPa and the parameter β in Eq. (26) was taken to be 3.0 [21]. Quarter symmetry was assumed where appropriate.

1. Construct Voronoi diagram from an initial set of nodes.
2. Construct shape functions, derivatives and smoothed values.
3. Build matrices and vectors for the optimization problem.
4. Solve the optimization problem to obtain a collapse load multiplier and displacement field data.
5. Calculate the local error for each Voronoi cell or node.
6. Calculate the global error (= sum of local errors).
7. If all local errors are smaller than the user-defined error tolerance δ then terminate as no further refinement is necessary.
8. Otherwise refine cells with a large local error and add new nodes.
9. Repeat from step 1.

The commercial interior point solver MOSEK [39], which is capable of rapidly solving large-scale mathematical optimization problems, was used to solve all optimization problems. Note that the high order shape functions used in the EFG method make *a priori* proof of the strict upper bound status of the solutions difficult. However, as the discretization is progressively refined using the adaptive procedure, increasingly close approximations of the true plastic collapse load multiplier can be expected to be obtained. Note also that a fixed number of adaptive steps (5) were performed for each problem in order to verify the performance of the procedure beyond the error threshold level likely to be used in practice to stop the procedure. Finally, note that in all examples a regular initial discretization of nodes was chosen for sake of simplicity and also to avoid potentially large estimated errors being identified in regions with a large maximum distance between neighbouring nodes, d_J^{max} (hence resulting in a large h_I, Eq. (26), and in turn potentially to unnecessary refinement).

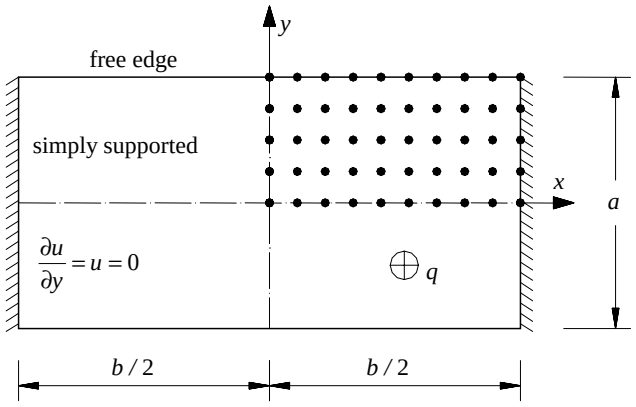

Fig. 5. Rectangular plate simply supported along 2 edges and subject to uniform pressure: geometry and initial nodal discretization (50 nodes over quarter of plate)

5.1 *Rectangular plate*

The first example considered comprises a rectangular plate, simply supported at two opposite edges and subjected to uniform out-of-plane pressure loading, as shown on Figure 5. The plate dimensions were set as $a = b/2 = 5$ m. In all cases a total of 10×5 nodes were initially used to discretize a quarter of the plate, as shown in Figure 5.

Firstly the threshold error tolerance δ was taken as 0.001 and the efficacy of the two refinement strategies illustrated in Figure 4 was investigated. Figure 6 shows the improvement in the computed collapse load as the problem is refined. It can be seen that adaptive strategy (I), which adds vertex nodes in Voronoi cells, results in a much better computed collapse load multiplier than strategy (II). This can be explained by the fact that the Voronoi cells are more regular with strategy (I) than with strategy (II); strategy (I) was therefore used in all subsequent computations described herein. The best solution found was 4.52 with 480 nodes, compared with 4.55 obtained using 648 nodes when using a uniform layout of nodes.

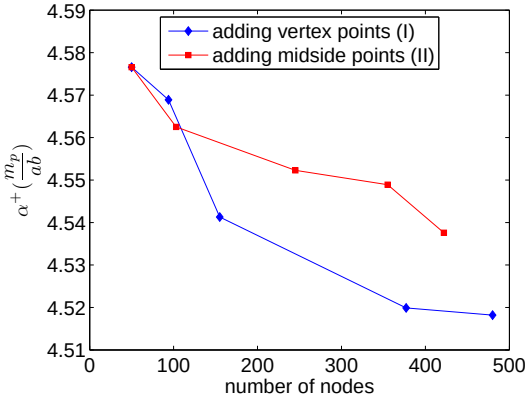

Fig. 6. Influence of adaptive strategy (I) and (II) on the computed load multiplier

The progress of the adaptive refinement procedure using strategy (I) is also shown graphically in Figure 7. What is clear is that the majority of nodes must be positioned in zones of plastic yielding in order to ensure that an accurate collapse load multiplier is obtained.

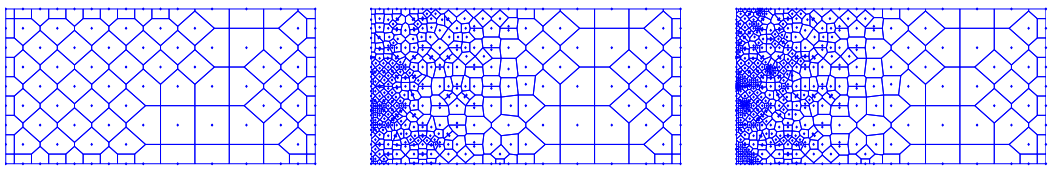

(a) Step 2, $\|e\| = 0.0109$ (b) Step 4, $\|e\| = 0.0097$ (c) Step 5, $\|e\| = 0.0044$

Fig. 7. Adaptive refinement using strategy (I) and $\delta = 0.001$ (rectangular plate)

Secondly the influence of the local error tolerance, in the range $0.0002 \leq \delta \leq$

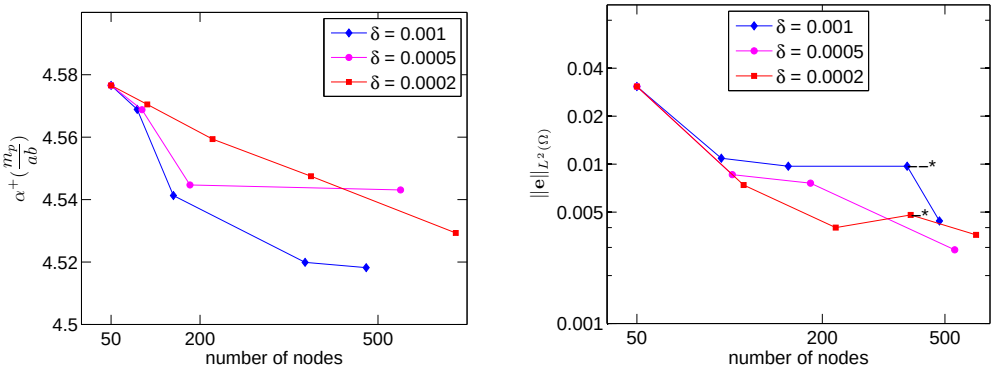

(a) Collapse load multiplier vs number of nodes

(b) Global error estimator vs number of nodes

Fig. 8. Influence of the error tolerance value δ (rectangular plate)
(*) - MOSEK solution status reported as either *Near-optimal* or *Unknown*

0.001, was investigated. Numerical collapse load multipliers and global error estimator values for various error tolerance values δ are shown in Figure 8 (where strategy (I) was used in all cases). It can be seen that the use of smaller tolerance values δ results in a higher computational cost, but does not always provide an improved computed collapse load multiplier. In other words, a 'good' continuous displacement field (i.e. one with a small associated error tolerance value) may not always provide a correspondingly 'good' collapse multiplier (see for example the case when $\delta = 0.005$ in Figure 8(a)); further investigations are required to more fully understand this issue.

5.2 L-shaped plate

The next example comprises an L-shaped plate subjected to a uniform load and with geometry and kinematic boundary conditions as shown in Figure 9. In all computations L was taken as 10 m and a total of 133 nodes were initially used to discretize the plate.

This problem was found to exhibit a singularity at the re-entrant corner, with a predicted yield line passing parallel to the supports from the re-entrant corner to the uppermost free edge. Computed collapse load multipliers and global error estimators for various different error tolerance values δ are plotted in Figure 10. It is evident from the two examples that a good estimate of the load multiplier could be obtained even when δ was taken as 0.001, despite the fact that the maximum number of nodes was in this case much smaller than when δ was taken as a lower value. This may be explained by the fact that in plastic regions error tolerance values greater than 0.001 are encountered, and nodes should be added in these zones. When δ is set to be smaller, a more *uniform* refinement is favoured, which affects efficiency. It is also shown in [20]

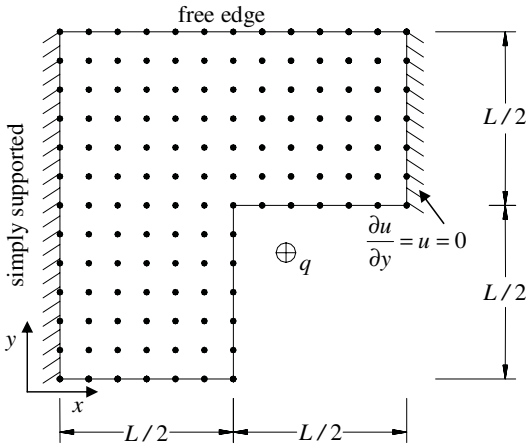

Fig. 9. L-shaped plate geometry and initial nodal discretization

that in some cases when δ is set close or equal to zero the global error estimator is surprisingly greater than when $\delta = 0.001$. The progress of the refinement is shown graphically in Figure 11. It is evident that errors are large in the zones near the re-entrant corner and emerging yield line, and consequently these areas are refined in each step of the adaptive scheme.

Table 1 illustrates the efficiency of the presented adaptivity scheme by comparing it with the uniform refinement strategy presented in [9]. It can be observed from the Table that the collapse multipliers obtained using the adaptive refinement scheme are lower than those obtained when using the uniform refinement strategy, despite the fact that the number of nodes (or variables) and CPU time used in the adaptive refinement scheme are both very much lower. e.g. The best upper-bound collapse multiplier was found to be 6.15 when a total of 453 nodes were present, which is considerably lower than the value of 6.298 obtained previously [9], when using up to 3816 nodes distributed uniformly across the plate. The best upper bound collapse multiplier obtained here is also lower than the solution of 6.289 obtained in [6], where up to 4900 HCT finite elements were used.

Uniform refinement [9]				Present adaptive refinement			
Nodes	variables	λ^+	CPU* (s)	Nodes	variables	λ^+	CPU* (s)
341	1705	6.79	6	133	665	7.02	2
645	3225	6.58	38	213	1065	6.62	3
1825	9125	6.38	171	318	1590	6.23	5
3816	19080	6.30	789	453	2265	6.15	14

*Mosek time taken to solve on a 2.8GHz Pentium 4 PC

Table 1
Comparison between load multipliers obtained using uniform and adaptive refinement strategies (L-shaped plate)

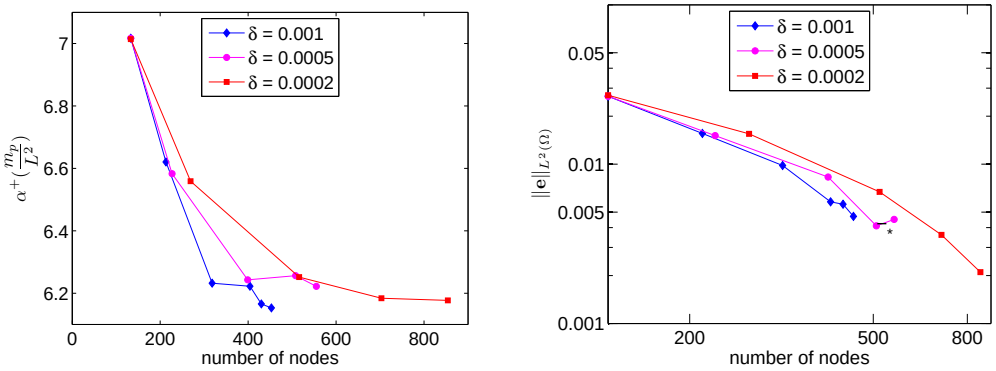

(a) Collapse load multiplier vs number of nodes

(b) Global error estimator vs number of nodes

Fig. 10. Influence of the error tolerance value δ (L-shaped plate)
(*) - MOSEK solution status reported as *Near-optimal*

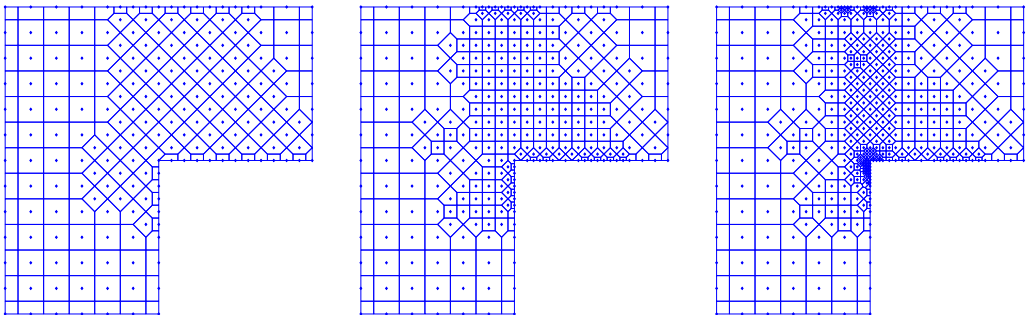

(a) Step 2 $\|e\| = 0.0156$ (b) Step 3 $\|e\| = 0.0058$ (c) Step 5 $\|e\| = 0.0047$

Fig. 11. Adaptive refinement with $\delta = 0.001$ (L-shaped plate)

5.3 Clamped circular plate

The third example involves a clamped circular plate with central concentrated load P. This problem exhibits a logarithmic singularity in the displacement field near the point load and has a known exact solution [40], $\alpha^+ = \frac{4\pi m_p}{\sqrt{3}P} = 7.255\,\frac{m_p}{P}$. The effectiveness of the proposed adaptive EFG method is demonstrated by comparing errors in the computed collapse load multiplier with and without nodal refinement; see Figure 12. In the adaptive analysis, δ was taken as 0.001 and strategy (I) was once again used. The best computed kinematic collapse load multiplier obtained was 7.27, which is just 0.2% higher than the exact solution. In the adaptive scheme the majority of the nodes were found to be concentrated in the zone around the singular point, as shown on Figure 13.

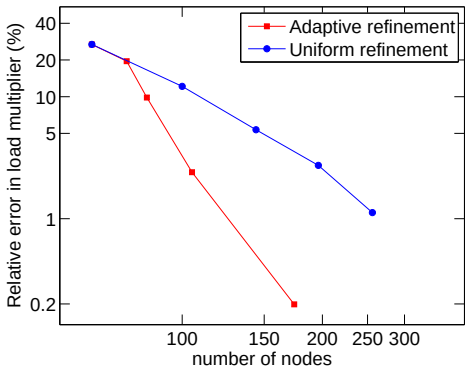

Fig. 12. Performance of uniform vs adaptive refinement schemes (circular plate)

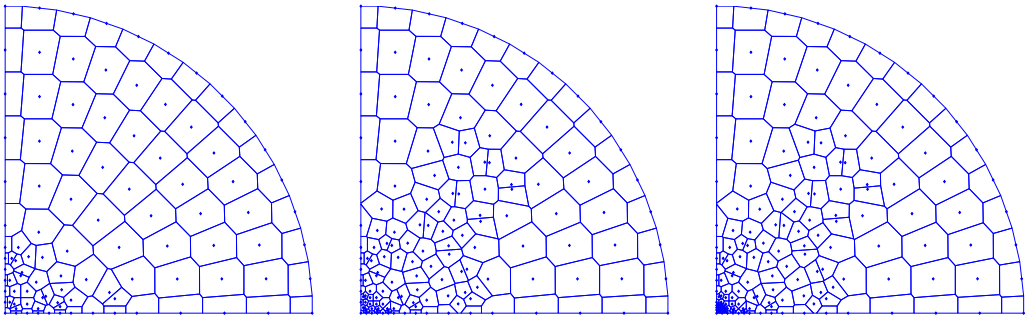

(a) Step 2 (b) Step 4 (c) Step 5

Fig. 13. Adaptive refinement (clamped circular plate)

5.4 Rectangular plate with eccentric square cutout

The last example involves a rectangular plate with an eccentric square cutout, of the same geometry as examined previously using an elasto-plastic model [41]. All external and internal edges are simply supported and the dimensions are shown in Figure 14. In the adaptive analysis, δ was taken as 0.001 and strategy (I) was once again used. Figure 15b shows a plot of the plastic dissipation for this problem. The implied yield line pattern shows good qualitative agreement with the result in [41]. Due to the dominance of the yield lines in the left part of the plate, most nodes were added in this area, as shown on Figure 15a. The best estimate of the collapse load multiplier was found to be 51.45 $\frac{m_p}{ab}$.

6 CONCLUSIONS

An efficient adaptive meshless limit analysis procedure for plates has been described. h-refinement is used and the smoothing technique used for nodal integration has been extended to allow error estimation at representative nodal cells, resulting in an efficient adaptive EFG method. For the plate problems

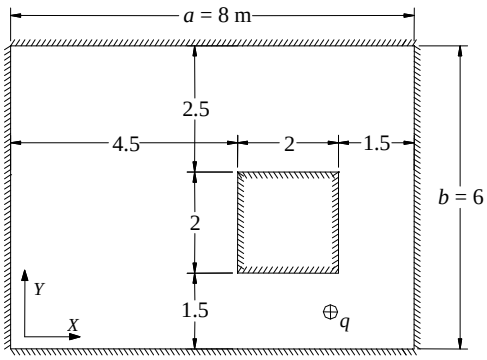

(a) Geometry and boundary conditions

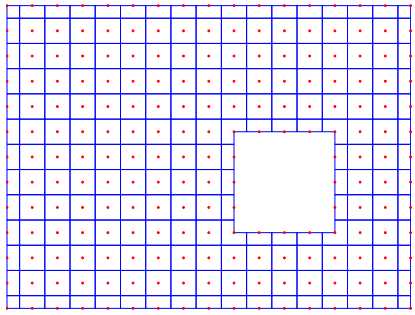

(b) Initial nodal discretization

Fig. 14. Details of rectangular plate with eccentric square cutout

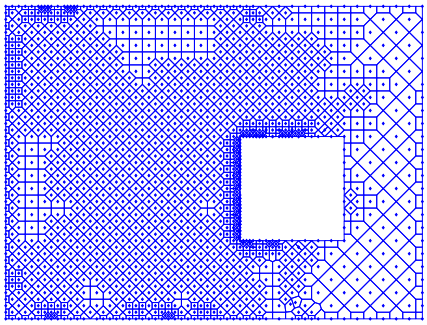

(a) Step 4: 1459 nodes

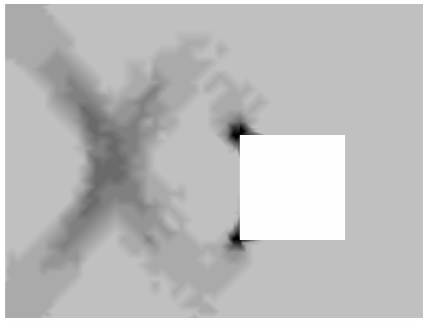

(b) Plastic dissipation distribution

Fig. 15. Adaptive refinement (rectangular plate with eccentric square cutout)

described here nodes were adaptively added at the vertices of Voronoi cells (termed strategy (I) in this paper), and an error tolerance value of $\delta = 0.001$ was used (however, since δ is a problem dependent parameter [21], numerical studies should be undertaken to determine its optimal value when tackling problems of a different type, e.g. plane strain, 3D etc.). Due to the naturally conforming properties of the meshfree approximation, the proposed adaptive scheme is conveniently performed without the need for complex manipulation of the data structures involved. Since properties of Voronoi cells are used as a reference for nodal addition strategies, irregular nodal layouts can be treated efficiently by the method. The adaptive scheme is able to capture yield line patterns arising from localized plastic deformations for problems of arbitrary geometry. It is found that the majority of nodes are concentrated in these plastic zones and that accurate estimates of the collapse load multiplier can be obtained using a relatively small number of nodes.

Acknowledgements

This research has been sponsored by the Ho Chi Minh City Government (300 Masters & Doctors Project) and the University of Sheffield. The third author acknowledges the support of EPSRC under grant reference GR/S53329/01.

References

[1] A. Makrodimopoulos, C. M. Martin, Upper bound limit analysis using simplex strain elements and second-order cone programming, International Journal for Numerical and Analytical Methods in Geomechanics 31 (2006) 835–865.

[2] M. Vicente da Silva, A. N. Antao, A non-linear programming method approach for upper bound limit analysis, International Journal for Numerical Methods in Engineering 72 (2007) 1192–1218.

[3] A. Capsoni, L. Corradi, Limit analysis of plates - a finite element formulation, Structural Engineering and Mechanics 8 (1999) 325–341.

[4] F. Tin-Loi, N. S. Ngo, Performance of the p-version finite element method for limit analysis, International Journal of Mechanical Sciences 45 (2003) 1149–1166.

[5] A. Chaaba, L. Bousshine, G. De Saxce, Kinematic limit analysis modelling by a regularization approach and finite element method, International Journal for Numerical Methods in Engineering 57 (2003) 1899–1922.

[6] C. V. Le, H. Nguyen-Xuan, H. Nguyen-Dang, Upper and lower bound limit analysis of plates using FEM and second-order cone programming, Computers and Structures 88 (2010) 65–73.

[7] C. V. Le, H. Nguyen-Xuan, H. Askes, S. Bordas, T. Rabczuk, H. Nguyen-Vinh, A cell-based smoothed finite element method for kinematic limit analysis, International Journal for Numerical Methods in Engineering (2010) accepted.

[8] S. Chen, Y. Liu, Z. Cen, Lower-bound limit analysis by using the EFG method and non-linear programming, International Journal for Numerical Methods in Engineering 74 (2008) 391–415.

[9] C. V. Le, M. Gilbert, H. Askes, Limit analysis of plates using the EFG method and second-order cone programming, International Journal for Numerical Methods in Engineering 78 (2009) 1532–1552.

[10] C. V. Le, M. Gilbert, H. Askes, Limit analysis of plates and slabs using a meshless equilibrium formulation, International Journal for Numerical Methods in Engineering (2010) accepted.

[11] K. Krabbenhoft, A. V. Lyamin, M. Hjiaj, S. W. Sloan, A new discontinuous upper bound limit analysis formulation, International Journal for Numerical Methods in Engineering 63 (2005) 1069–1088.

[12] C. C. Smith, M. Gilbert, Application of Discontinuity Layout Optimization to Plane Plasticity Problems, Proceedings of the Royal Society A 463 (2007) 2461–2484.

[13] L. A. Borges, N. Zouain, C. Costa, R. Feijoo, An adaptive approach to limit analysis, International Journal of Solids and Structures 38 (2001) 1707–1720.

[14] E. Christiansen, O. S. Pedersen, Automatic mesh refinement in limit analysis, International Journal for Numerical Methods in Engineering 50 (2001) 1331–1346.

[15] A. V. Lyamin, S. W. Sloan, K. Krabbenhoft, M. Hjiaj, Lower bound limit analysis with adaptive remeshing, International Journal for Numerical Methods in Engineering 63 (2005) 1961–1974.

[16] H. Ciria, J. Peraire, J. Bonet, Mesh adaptive computation of upper and lower bounds in limit analysis, International Journal for Numerical Methods in Engineering 75 (2008) 899–944.

[17] J. Munoz, J. Bonet, A. Huerta, J. Peraire, Upper and lower bounds in limit analysis: adaptive meshing strategies and discontinuous loading, International Journal for Numerical Methods in Engineering 77 (2009) 471–501.

[18] H. J. Chung, T. Belytschko, An error estimate in the EFG method, Computational Mechanics 21 (1998) 91–100.

[19] G. R. Liu, Z. H. Tu, An adaptive procedure based on background cells for meshless methods, Computer Methods in Applied Mechanics and Engineering 191 (2002) 1923–1943.

[20] U. Haussler-Combe, C. Korn, An adaptive approach with the Element-Free-Galerkin method, Computer Methods in Applied Mechanics and Engineering 162 (1998) 203–222.

[21] T. Rabczuk, T. Belytschko, Adaptivity for structured meshfree particle methods in 2D and 3D, International Journal for Numerical Methods in Engineering 63 (2005) 1559–1582.

[22] Y. You, J.S. Chen, H. Lu, Filters, reproducing kernel, and adaptive meshfree method, Computational Mechanics 31 (2003) 316–326.

[23] J. Yvonnet, G. Coffignal, D. Ryckelynck, Ph. Lorong, F. Chinesta, A simple error indicator for meshfree methods based on natural neighbors, Computers and Structures 84 (2006) 1301–1312.

[24] W. K. Liu, S. Li, T. Belytschko, Moving least-square reproducing kernel methods (I) methodology and convergence, Computer Methods in Applied Mechanics and Engineering 143 (1997) 113–154.

[25] Y. Krongauz, T. Belytschko, Consistent pseudo-derivatives in meshless methods, Computer Methods in Applied Mechanics and Engineering 146 (1997) 371–386.

[26] S. Beissel, T. Belytschko, Nodal integration of the element-free Galerkin method, Computer Methods in Applied Mechanics and Engineering 139 (1996) 49–74.

[27] J. Bonet, S. Kulasegaram, Correction and stabilization of smooth particle hydrodynamics methods with applications in metal forming simulations, International Journal for Numerical Methods in Engineering 47 (2000) 1189–1214.

[28] J. S. Chen, C. T. Wu, S. Yoon, Y. You, A stabilized conforming nodal integration for Galerkin mesh-free methods, International Journal for Numerical Methods in Engineering 50 (2001) 435–466.

[29] T. Rabczuk, T. Belytschko, S.P. Xiao, Stable particle methods based on lagrangian kernels, Computer Methods in Applied Mechanics and Engineering 193 (2004) 1035–1063.

[30] M. A. Puso, J. S. Chen, E. Zywicz, W. Elmer, Meshfree and finite element nodal integration methods, International Journal for Numerical Methods in Engineering 74 (2008) 416–446.

[31] T. P. Fries, T. Belytschko, Convergence and stabilization of stress-point integration in mesh-free and particle methods, International Journal for Numerical Methods in Engineering 78 (2008) 1067–1087.

[32] Q. Duan, T. Belytschko, Gradient and dilatational stabilizations for stress-point integration in the element-free Galerkin method, International Journal for Numerical Methods in Engineering 77 (2009) 776–798.

[33] K. Y. Sze, J. S. Chen, N. Sheng, X. H. Liu, Stabilized conforming nodal integration: exactness and variational justification, Finite Elements in Analysis and Design 41 (2004) 147–171.

[34] D. Wang, J. S. Chen, Locking-free stabilized conforming nodal integration for meshfree Mindlin-Reissner plate formulation, Computer Methods in Applied Mechanics and Engineering 193 (2004) 1065–1083.

[35] J. W. Yoo, B. Moran, J. S. Chen, Stabilized conforming nodal integration in the natural-element method, International Journal for Numerical Methods in Engineering 60 (2004) 861–890.

[36] T. Belytschko, Y. Y Lu, L. Gu, Element-Free Galerkin methods, International Journal for Numerical Methods in Engineering 37 (1994) 229–256.

[37] P. V. Nguyen, T. Rabczuk, S. Bordas, M. Duflot, Meshless methods: A review and computer implementation aspects, Mathematics and Computers in Simulation 79 (2008) 763–813.

[38] P. Krysl, T. Belytschko, Analysis of thin plates by the Element-Free Galerkin method, Computational Mechanics 17 (1995) 26–35.

[39] Mosek, The MOSEK optimization toolbox for MATLAB manual, version 5.0. http://www.mosek.com, Mosek ApS (2008).

[40] H.G. Hopkins, A.J. Wang, Load-carrying capacities for circular plates of perfectly-plastic material with arbitrary yield condition, Journal of the Mechanics and Physics of Solids 3 (1954) 117–129.

[41] H. Askes, A. Rodriguez-Ferran, A. Huerta, Adaptive analysis of yield line patterns in plates with the arbitrary Lagrangian-Eulerian method, Computers and Structures 70 (1999) 257–271.